Sindh Univ. Res. Jour. (Sci. Ser.) Vol. 41 (2) 93-98 (2009)

Sindh Univ. Res. Jour.

SURJ

FINITE ELEMENT SIMULATION OF NEWTONIAN FLOWS PAST AN IRREGULAR SOLID OBSTACLE

A. A. Shaikh, F. Shah, and M.S. Chandio

Department of Basic Sciences, Mehran University of Engineering and Technology, Jamshoro
(Received 02nd October 2009 and Revised 06th November 2009)

Abstract

Finite element simulation of viscous flow past a triangular shape solid obstacle is studied here. The liquid for simulation is considered here to be Newtonian. The shearing effects of the surrounding fluid on the solid obstacle are taken into account as well as pressure. Finite element Semi implicit time-stepping Taylor/Galerkin Pressure Correction Scheme is employed here. Incompressible and isothermal fluid flow problem is studied. Both coarse and dense structured meshes are used to investigate the accuracy, stability and consistency of the numerical scheme. Numerical results show the potentialities of the numerical method.

Keywords: Finite Element Simulation, Solid Obstacle, Newtonian flow, structured meshes.

1. Introduction

The numerical study of channel flow of Newtonian and Non-Newtonian fluids past a solid obstacle is significant to many industrial problems. Various methods such as experimental, mathematical analysis and numerical simulation are employed for studying the behaviour of such fluid flow problems past an irregular obstacle (Matallah, *et al*.,1998 and Aboubakar, *et al*., 2002).

The industrial problems frequently encounter mixing and moulding processes in many applications, and the quality of the resulting mixture directly affects the quality of the finished product. The flow past a solid obstacle is related to industrial problems. Both, Newtonian and viscoelastic fluids are used in applications involving flows around solid obstacles such as triangle or trapezium. Since the moulding improves the design and functionality of the end-product, so the industrial applications of such type may contain the solid obstacles mould to form a finished product.

The Numerical Simulation of flow past an irregular solid obstacle for viscous and viscoelastic fluids is rarely simulated due to the involved irregular solid surfaces.

The abrupt changes of geometry with singularities may generate high level of shearing stresses for a viscoelastic fluid, which may cause numerical instabilities and lead to divergence at high Deborah numbers (Dou and Phan-Thien, 1999).

Various finite element methods have been proposed to deal with such type of problems. These methods have the advantage of easily generating triangular meshes fitted with propagating irregular interfaces. These methods are adopted in most numerical studies on Newtonian and non-Newtonian flows past a sphere, a cylinder, or annular flow between two eccentric cylinders, and the sentation or fluidization of many solid particles, see for more details (Aboubacar *et al*., 2002 and Haung *et al*.,1998 Oliveria and Pinho, 1999 and Dou and Phan-Thein, 1999).

The purpose of this work is to examine the potentialities of a proposed time-splitting numerical scheme in order to compute flow past an irregular solid obstacle in two-dimensions.

* Institute of Mathematics and Computer Science, University of Sindh, Jamshoro.

The laminar flow of viscous fluid is considered here. Triangular structured meshes are used for numerical simulation. The problem is relevant with flow past an irregular solid obstacle. Finite element Semi implicit time-stepping Taylor/Galerkin Pressure Correction Scheme is employed, (Townsend and Webster, 1987 Carew, *et al*., 1999, Hawken *et al*., 1990).

2. Governing Equations

In the absence of body forces, the momentum and the continuity equations may be described as:

$$\rho \frac{\partial \mathrm{u}}{\partial t} = \nabla . T - \rho \mathrm{u}.\nabla \mathrm{u} - \nabla p \qquad (1)$$

$$\nabla . \mathrm{u} = 0 \qquad (2)$$

where $\boldsymbol{T}$ is the stress tensor, ρ is the fluid density, *t* is the time, u(x,t) is the fluid velocity and p is the isotropic pressure. For Newtonian fluid, the stress tensor $\boldsymbol{T} = 2\mu \mathrm{D}$**.**

Here, the rate of deformation tensor *D* is described as follow*:*

$$\mathrm{D} = \frac{\mathrm{L} + \mathrm{L}^{\mathrm{t}}}{2} \quad \text{and} \quad \mathrm{L}^{\mathrm{t}} = \nabla \mathrm{u} .$$

With a constant viscosity and using the continuity equation (2), the Navier-Stokes equation can be recovered,

$$\rho \frac{\partial \mathrm{u}}{\partial t} = \mu \nabla^2 \mathrm{u} - \rho \, \mathrm{u}.\nabla \mathrm{u} - \nabla p \qquad (3)$$

where $\mu \nabla^2 \mathrm{u}$ is the diffusion term.

Adopting characteristic scales for velocity and pressure, an equivalent non-dimensional system of equations can be expressed as follow:

$$\mathrm{Re} \frac{\partial \mathrm{u}}{\partial t} = \nabla^2 \mathrm{u} - \mathrm{Re}\, \mathrm{u}.\nabla \mathrm{u} - \nabla p \, , \qquad (4)$$

$$\nabla . \mathrm{u} = 0, \qquad (5)$$

where the non-dimensional group Reynolds number is defined as $Re = \frac{\rho U L}{\mu}$.

4. Finite Element Analysis

For the solution of governing equations (4) and (5), we have used Semi-Implicit Taylor- Galerkin - Pressure-Correction algorithm. Adopting the notation of Cuvelier *et al.,*(1992). on the velocity ($\mathrm{U}(\mathbf{x},t) = \mathrm{U}^j(t)\ \phi_j(\mathbf{x})$) and pressure ($\mathrm{P}(\mathbf{x},t) = \mathrm{P}^k(t)\ \varphi_k(\mathbf{x})$) fields on the specified domain, the fully discrete semi-implicit Taylor-Galerkin/pressure-correction system of equations in matrix form is given as follow:

Stage 1a:

$$(\frac{2\,\mathrm{Re}}{\Delta t} M + \frac{1}{2} S)(U^{n+\frac{1}{2}} + U^n) = \{-[S + \mathrm{Re}\, N(U)]U + L^T P\}^n$$

Stage 1b:

$$(\frac{\mathrm{Re}}{\Delta t} M + \frac{1}{2} S)(U^* - U^n) = (-[SU + L^T P]^n - [\mathrm{Re} N(U)U]^{n+\frac{1}{2}}$$

Stage 2:

$$K(P^{n+1} - P^n) = -\frac{2}{\Delta t} L U^*$$

Stage 3:

$$\frac{1}{\Delta t} M(U^{n+1} - U^*) = \frac{1}{2} L^T (P^{n+1} - P^n)$$

where *M*, *S*, *N(U), L,* and *K* are consistent mass matrix, momentum diffusion matrix, convection matrix , pressure gradient matrix and pressure stiffness matrix respectively. In matrix form, these can be expressed as follow:

$$M_{ij} = \int_\Omega \phi_i \phi_j \, d\Omega,$$

$$N(U)_{ij} = \int_\Omega \phi_i (\phi_l U_l \frac{\partial \phi_j}{\partial x} + \phi_l U_l \frac{\partial \phi_j}{\partial y}) \, d\Omega,$$

$$((L_k)_{ij}) = \int_\Omega \frac{\partial \phi_j}{\partial x_k} \, d\Omega,$$

$$K_{ij} = \int_\Omega \nabla \psi_i \, \nabla \psi_j \, d\Omega,$$

$$S_{ij} = \int_\Omega \nabla \phi_i \, \nabla \phi_j \, d\Omega$$

System of linear equations is solved by iterative Jacobis method and by direct

Choleski method (for pressure). The details upon this implementation may be found in (Townsend and Webster 1987 and Hawken *et al*., 1990 and Chandio and Webster 2002).

5. Problem Description

A straight pipe with half triangular solid obstacle on the inner surface of the pipe is considered here, see (**Fig. 1**). The ratio of the obstacle is taken as R_b/R_t = 0.2. The zoomed version of the triangular solid obstacle is shown in (**Fig. 2**).

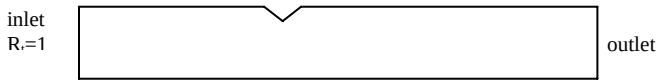


Fig. 1. Problem Geometry

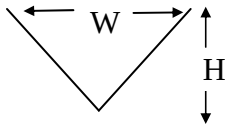


Fig. 2. Zoomed geometry of half-triangular solid obstacle

Boundary Conditions on the Walls

No slip boundary conditions, *i.e.* u=v=0 are imposed on the solid boundaries.

Inlet Boundary conditions

Parabolic velocity profile is imposed in this region, which can be expressed as

$$U=U_{max}\,[1-(y/Y)^2]$$

where y is distance of point along Y-axis and Y is radius and taken of unit length. Thus we obtained maximum velocity at the inlet as follow:

$$U_{max} = (1 - y^2)$$

Outlet Boundary Conditions

On the outlet, continuative boundary conditions are considered, which can be expressed as

$u_x = v_x = 0$.

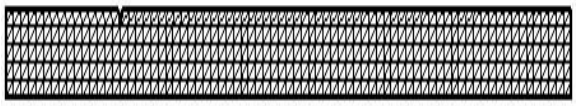
6. Results and Discussions

In the application of Finite Element analysis, one of the most important decisions is to design the mesh, so that the mesh should be sufficiently fine in the area of interest in order to capture the solution accurately. We have used three different meshes, 5x175, 10x75 and 30x150, in order to capture the accuracy of the variables of interest.

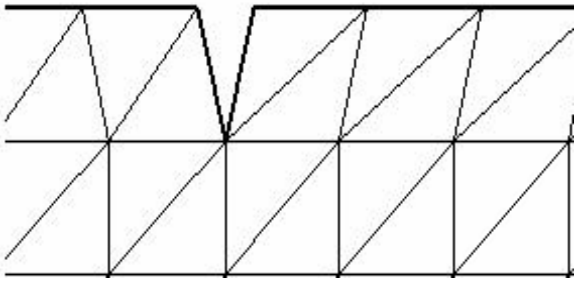
Here, flow past a triangular shape solid obstacle, which is chinning on the inner wall of straight tube, is under investigation. In figure 2, a zoomed geometry of the solid obstacle is depicted, where W and H are the underside width and height of the isosceles triangle respectively.

The underside width and height of the triangular obstacle is taken respectively as W = $2R_b$ and H=$0.8R_b$ and the blockage ratio is taken as R_b/R_t = 0.2 as proposed by Yang and Mao, (2003).

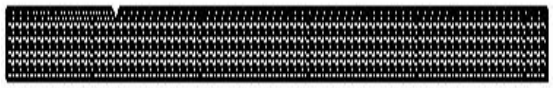
Structured triangular meshes of 5x75 having 750 elements and 1663 nodes, 10x75 having 1500 elements and 3175 nodes and 30x150 having 9000 elements and 18373 nodes, see(**Fig. 3, a,b. 4, a,b, 5, a,b.**).



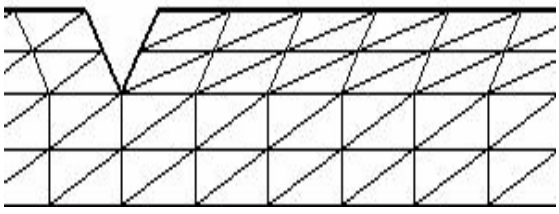
(a) Full mesh



(b) Zoomed mesh near the obstacle
Fig. 3: mesh 5x75



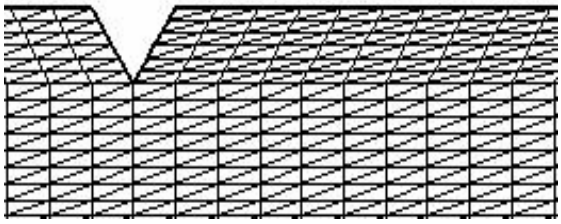
(a) Full mesh



(b) Zoomed mesh near the obstacle
Fig. 4: mesh 10x75



(a) Full mesh

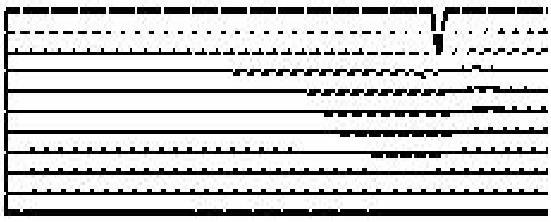


(b) Zoomed mesh near the obstacle
Fig. 5: mesh 30x150

Since the problem under investigation is symmetric, so the numerical results are obtained using upper half of the tube.

In the first instance numerical results are obtained using, a coarse mesh 5x75.

In (**Fig. 6, a,b**). Velocity vectors are shown. A parabolic profile is observed at the inlet. A similar trend is seen at the outlet that guarantees the accuracy, consistency and stability of the numerical scheme in the presence of irregular solid obstacle. The maximum pressure is observed at the inlet and near the obstacle while hitting the fluid with it, see (**Fig. 7**).



(a) Inlet velocity vectors profile



(b) Outlet velocity vectors profile
Fig. 6: mesh 5x75, velocity vectors

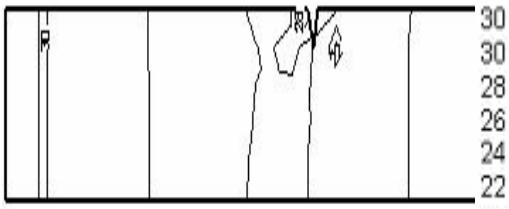


Fig. 7: mesh 5x75, Pressure contours, maximum pressure at the inlet and near the obstacle

The maximum shear rate occurs past the solid obstacle, see (**Fig. 8**). A similar level of pressure and shear rate is observed using mesh 10x75. Thus, no change is observed shifting from mesh 5x75 to 10x75, see (**Fig. 9-10**).



Fig. 8: mesh 5x75, Shear rate, maximum shear-rate below the obstacle



Fig. 9: mesh 10x75, Pressure contours, maximum pressure at the inlet and near the obstacle

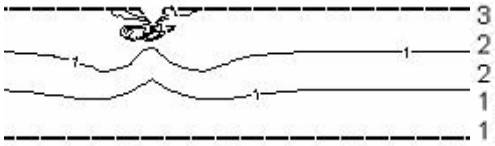


Fig. 10: mesh 10x75, Shear rate, maximum shear-rate below the obstacle

The fluid passing through the narrow gap below the obstacle generates high shear rates that may cause instabilities in the numerical simulation. However, the level of pressure remains same as of coarse meshes (5x75 and 10x75), see (**Fig. 11**). The level of shear rates have slightly increased using dense mesh 30x150, see (**Fig. 12**). Velocity vectors below the obstacle depicts vortex that causes shear rates, see (**Fig. 13**).



Fig. 11: mesh 30x150, Pressure contours, maximum pressure at the inlet and near the obstacle

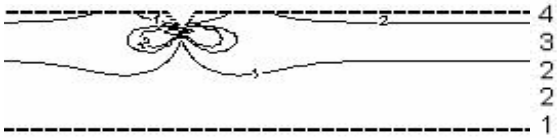


Fig. 12: mesh 30x150, Shear rates, maximum shear-rate below the obstacle

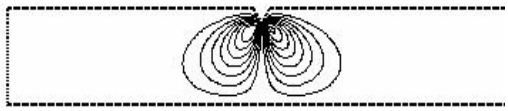


Fig. 13: mesh 30x150, velocity, *v*, contours around the obstacle.

7. Conclusion

In the present study, Newtonian fluid is considered for the numerical results. Here, we found that the maximum pressure exists at the inlet and near the obstacle for all meshes. The velocity vectors show parabolic profile at the inlet and outlet, that guarantees the accuracy of the numerical scheme in the presence of solid obstacle. The accurate measurement of shear stress is of importance in mixing flows. In order to capture the accurate levels of shear rates, three different meshes are used for numerical computation. We observed that the level of shear rates increases from coarse meshes to dense meshes. In the present study it is observed that triangular meshes capture the solution accuracy. Future studies will focus upon non-Newtonian flows past an irregular solid obstacle and comparison among Newtonian and non-Newtonian flow behavior.

References

Aboubaca, M., H. Matallah, H. R. Tamaddon-Jahromi and M. F. Webster (2002) *Numerical prediction of extensional flows in contraction geometries: hybrid finite volume/ element method"*, J. Non-Newt. Fluid Mech., vol. (**104**): 125-164.

Carew, E.O.A., P. Townsend and M.F. Webster, (1993) *A Taylor-Petrov-Galerkin algorithm for viscoelastic flow*, J. non-Newt. Fluid Mech., vol. (**50**): 253-287.

Chandio, M. S. and M. F. Webster, (2002) *Numerical simulation of viscous free-surface flows for reverse roller-coating,* Int. J. Numer. Meth. Heat Fluid Flow, vol. (**12**): 434-457.

Cuvelier C., A. Segal and A. A. Van Steenhoven (1992) *Finite Element methods and Navier-Stokes equation D. Reidel* Publishing Company.

Dou, H., and N. S. Phan-Thien, (1999) *The flow of an Oldroyd-B fluid past a cylinder in a channel: adaptive viscosity vorticity (DAVSS-ω) formulation*, J. Non-Newt. Fluid Mechs., vol. (87): 47-73.

Hawken, D.M., H.R. Tamaddon-Jahromi, P. Townsend, and M.F. Webster, (1990) *A Taylor-Galerkin Based Algorithm for viscous incompressible flow*, Int. J. Num. Meth. Fluids, vol. (10): 327-351.

Huang, P.Y., H.H. Hu, and D.D. Joseph, (1998), *Direct simulation of sedimentation of elliptic particles in Oldroyd B fluids*, J. Fluid Mechs., vol. (362): 297-326.

Matallah, M., P. Townsend, and M.F. Webster, (1998) *Recovery and stress-splitting schemes for viscoelastic flows*, J. non-Newt. Fluid Mech., vol. (**75**): 139-166.

Paulo J. Oliveria, and T. Fernando Pinho, (1999) *Analytical solution for fully developed channel and pipe flow of Phan–Thien-Tanner fluids*", J. Fluid Mech., vol. (**387**): 271-280.

Townsend, P. and M. F. Webster, (1987) *An Algorithm for the Three-Dimensional Transient Simulation of non-Newt. Fluid Flows*, Proc. NUMETA 87, Martinus Nijhoff, Publishers, Dordrecht, (**2**): T12/1.

YANG, Chao and Mao, Zia-Sha, (2003) *Numerical Simulation of Viscous Flow of A Non-Newtonian Fluid Past an Irregular Solid obstacle By The Mirror Fluid Method,* Third International Conference on CFD in minerals and process industries CSIRO, Melbourne, Austrlia, Commmonwealth Scientific and Industrial Research Organization 391-396.